

Journal of volcanology and geothermal research

Journal of Volcanology and Geothermal Research 114 (2002) 313-330

www.elsevier.com/locate/jvolgeores

## Structural origin of large gas cavities in the Big Obsidian Flow, Newberry Volcano

Jonathan Castro a,\*, Katharine Cashman b, Nick Joslin b, Brian Olmsted c

a Department of Geology, Oberlin College, Oberlin, OH 44074-1044, USA b Department of Geological Sciences, University of Oregon, Eugene, OR 97403-1272, USA <sup>c</sup> Department of Earth and Environmental Science, New Mexico Tech, Socorro, NM 87801, USA

Received 22 August 2000; received in revised form 10 July 2001; accepted 10 July 2001

#### **Abstract**

Mesoscopic structures in four large cavities on the Big Obsidian Flow, OR, USA, provide evidence of links between large-scale surface folding, cavity formation, and hazardous explosive activity originating from within the flow. Stereographic analysis of flow banding, stretched bubble lineation, striations, and mesoscopic fold axes indicates that three of the cavities are near-cylindrical folds. Cavity fold axes are oriented parallel to large-scale compressional flow ridge axes, suggesting that cavities form in response to shortening during flow advance. Large surface folds develop as the upper 10 m of the cooler flow surface buckles when the flow front cools, slows, and stalls against topographic barriers. Void space is created in fold hinges as obsidian layers shear past each other and pull apart. The resultant cavities may serve as reservoirs for exsolved volatiles or surface water which may later vent explosively to form explosion craters on the flow surface. © 2002 Elsevier Science B.V. All rights reserved.

Keywords: obsidian; gas cavity; explosion craters; folding

#### 1. Introduction

Analysis of structures preserved in obsidian flows aids in the interpretation of flow emplacement (e.g. Fink and Fletcher, 1978; Fink, 1980, 1983; Smith and Houston, 1994). Macroscopic and mesoscopic features of obsidian flows reflect the complex rheology of the variably vesicular rhyolite that comprises these unusual flows, and

Castro and Cashman, 1999). Also unusual is the prevalence of explosion craters on the surface of several Holocene obsidian flows (e.g. Big and Little Glass Mountains, Big Obsidian Flow, Rock Mesa Obsidian Flow). As these features demonstrate, surficial explosive activity may pose unique hazards associated with the emplacement of obsidian lavas (e.g. Fink and Manley, 1989; Fink et al., 1992).

have been studied in this context (Fink, 1980;

Large cavities found within some explosion craters in the Big Obsidian Flow, OR, USA, were originally interpreted as 'giant gas bubbles' (Jensen, 1993) formed by exsolution, diffusion, and buoyant rise of magmatic volatiles within the

Tel.: +1-440-775-6701; Fax: +1-440-775-8886. E-mail addresses: jon.castro@oberlin.edu (J. Castro),

cashman@oregon.uoregon.edu (K. Cashman),

bolmsted@nmt.edu (B. Olmsted).

<sup>\*</sup> Corresponding author.

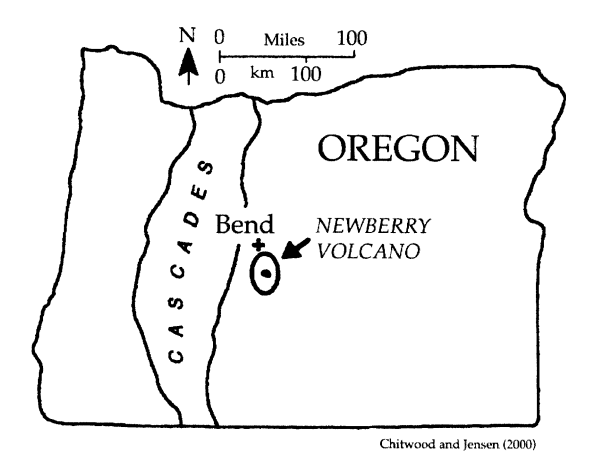


Fig. 1. Location map of Newberry Volcano, OR, USA (from Chitwood and Jensen, 2000).

flow. Jensen (1993) suggested that as pressure within each bubble increased and exceeded the strength of overlying lava, the gas bubbles vented explosively to form craters on the surface. This mechanism of cavity formation would suggest that explosion craters could form after flow advance had ceased. An alternative explanation is that cavity formation is intimately associated with flow advance, and thus that hazards posed

by cavity formation are more likely to accompany flow emplacement.

Here we analyze the structural characteristics of mesoscopic flow features found within four large cavities exposed on the surface of the Big Obsidian Flow at Newberry Volcano, OR, USA (Fig. 1). These structural elements suggest a genetic link between explosive cratering and deformation acquired during flow advance. Below we present measurements of flow banding, folds, stretched bubble lineation, and striations that relate cavity formation to buckling of obsidian layers during flow advance. Such voids could serve as reservoirs for exsolved magmatic and meteoric volatiles, and may vent explosively to form craters on the flow surface. While this type of surficial explosive activity has not been recognized in recent and currently active silicic domes (e.g. Nakada et al., 1995), it represents an important volcanic hazard common in more evolved, rhyolitic obsidian flows.

#### 2. Geologic background

The Big Obsidian Flow erupted approximately 1300 yr ago from the summit caldera of Newberry

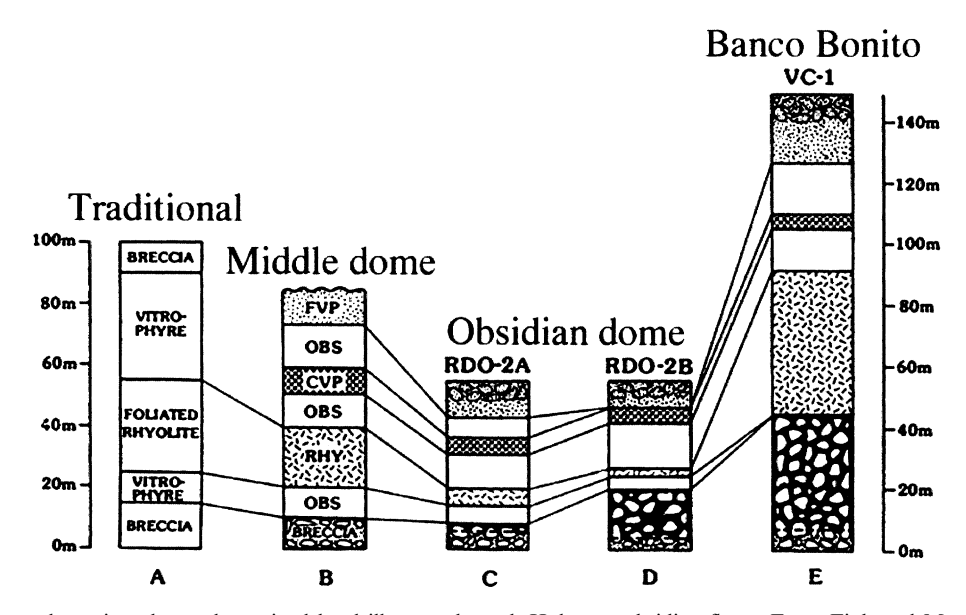


Fig. 2. Textural stratigraphy as determined by drill cores through Holocene obsidian flows. From Fink and Manley (1987).

Volcano (Robinson and Trimble, 1983). The eruption began with a phase of explosive activity that deposited pumice and dense lava blocks ( $\leq 1$  m in diameter) within the caldera. Approximately 0.32 km³ of tephra was erupted and deposited as far east as Idaho (MacLeod et al., 1982). Eruptions of pyroclastic flows into Paulina Lake preceded a final stage of effusive activity in which the 0.13-km³ Big Obsidian Flow was emplaced. The Big Obsidian Flow is about 1.8 km long and locally thicker than 30 m.

Like many Holocene obsidian flows throughout the western USA, the Big Obsidian Flow consists of four end-member lava types: finely vesicular pumice (FVP), coarsely vesicular pumice (CVP), obsidian, and vent-facies rhyolite. Based on flow front exposures and textural analyses of drill core samples, Fink and Manley (1987) suggested a general obsidian flow stratigraphy consisting of a basal breccia that is overlain by dense obsidian, CVP, an uppermost obsidian layer, and a flow surface of brecciated FVP (Fig. 2). This stratigraphy can be seen in the upper 15 m of the Big Obsidian Flow, with an additional textural unit of vent-facies rhyolite restricted to the southernmost extent of the Big Obsidian Flow, where it



Fig. 3. Aerial photograph mosaic of the Big Obsidian Flow showing arcuate flow ridges concave toward the vent. Dark lava is CVP while light gray lava is FVP. Scale bar represents approximately 300 m.



Fig. 4. Explosion crater on the surface of the Big Obsidian Flow. Pit is approximately 15 m in diameter and 10 m deep. Cavity A (not visible) is located in the bottom of the crater. Note rim of ejecta shown in the lower right corner of photograph.

forms an elevated domal protrusion that marks the vent. The basal sections of the flow are obscured by talus.

The Big Obsidian Flow surface has numerous regularly spaced arcuate ridges and intervening cuspate valleys. Fink (1980) interpreted similar structures on Big Glass Mountain to be folds formed by buckling of the upper surface during flow advance (Fig. 3), in response to compression parallel to the flow direction. Creation of these structures requires the viscosity of the flow surface to be substantially greater than that of the flow interior (Fink and Fletcher, 1978; Fink, 1980). As in the development of pahoehoe ropes on basaltic lava surfaces, folds form when the rate of flow front advance is less than the flow rate from the vent. Flow of lava from the vent compresses the surface, which buckles into a series of folds whose wavelengths are proportional to the crust thickness and ratio of viscosity of the surface crust to that of the flow interior.

In addition to folds, obsidian flow surfaces are commonly marked by explosion craters (Fig. 4; Jensen, 1993), conical depressions in the flow sur-

face that are typically 10-25 m in diameter, and 5-15 m deep. Some of these craters are underlain by cavities. Russell (1905) first described explosion craters as 'depressions where explosions occurred', in recognition of their outer concentric rings of coarse grained (0.1-1 m) obsidian and pumice. Such ejecta deposits are absent from known collapse depressions or inflation cavities on basaltic flows (Green and Short, 1971; Hon et al., 1994), and imply an origin by gas pressure build-up. It is not clear whether the gas driving these explosions is purely magmatic (e.g. Jensen, 1993) or whether they could have a phreatic component (e.g. Mastin, 1995; Moyer and Swanson, 1987). For this reason, it is important to understand the origin of the underlying cavity structures.

#### 3. Methods

We analyzed three large voids located in the bottoms of explosion craters X, G, and A. Each of these cavities is referred to by the same label

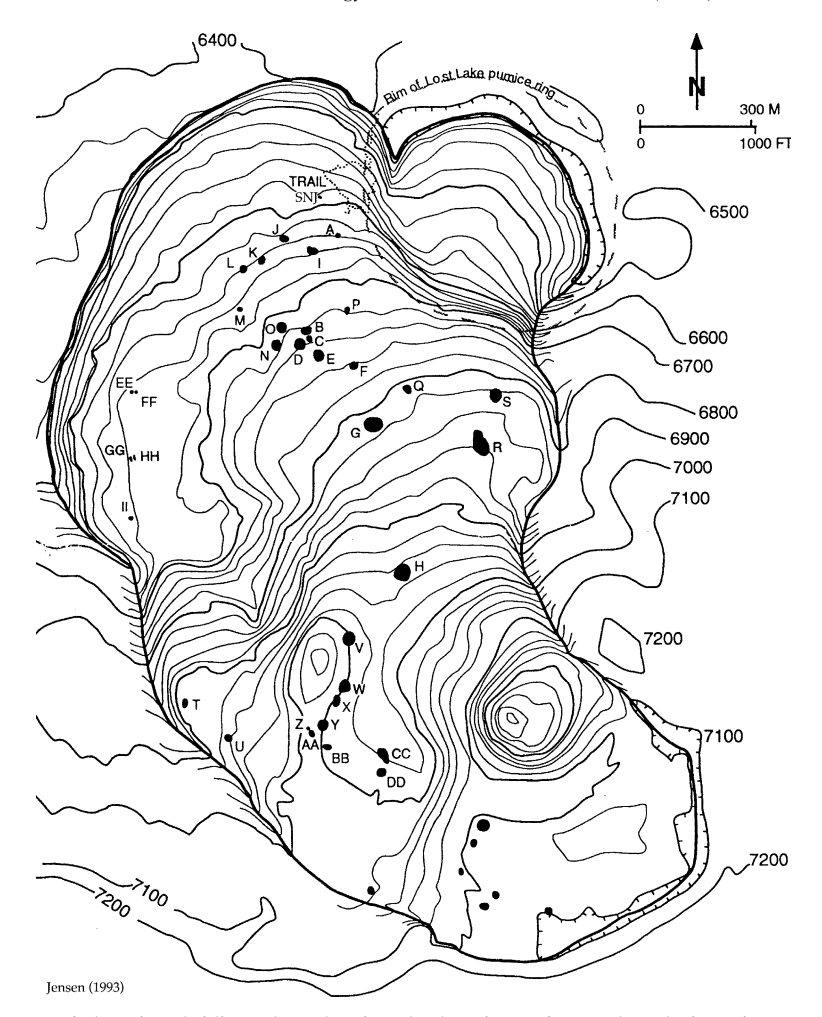


Fig. 5. Topographic map of the Big Obsidian Flow showing the locations of several explosion pits mapped by Jensen (1993). Cavities X, G, and A occur in explosion pits of the same designation. Cavity structure SNJ (near 'TRAIL' on north end of flow) is not associated with an explosion pit.

as the crater name (Fig. 5). In addition, we measured structures in one small cavity (SNJ) not associated with an explosion crater. Cavity SNJ is exposed by a large fracture trending approximately east—west and shows no evidence of explosive venting.

We measured structural features exposed in the four cavities, and surveyed cavity A to constrain its three-dimensional shape and size. Structural measurements included strike and dip of flow banding, trend and plunge of lineations and striations in the plane of banding, and trend and plunge of fold axes. Surveying was conducted

with a Wild Electronic Distance Measurer model TS-1600. Measurement precision is ±1 cm.

#### 4. Results

Cavities are typically 5–15 m in length, and are antiformal in cross section (Fig. 6). Cavity morphology varies from cylindrical to dome-shaped. Most cavity walls are formed by dense, flowbanded obsidian ranging in thickness from 0.1–3 m, although one cavity (cavity X) is composed of two separate walls that bound the eastern and





Fig. 6. Cavity structures SNJ (top) and G (bottom). Both features exhibit flow-layered obsidian walls. Lineations and striations in cavity G are evident in the left center part of the photograph.

western edges of a large explosion crater (Fig. 7). Of the four cavities that we studied, two (A and SNJ) are overlain by CVP, while the other two (X and G) are associated only with spines of obsidian.

## 4.1. Structures preserved in cavities

Cavity walls preserve mesoscopic structures such as folds, stretched vesicle lineations, flow banding, chatter marks, and striations (Table 1).

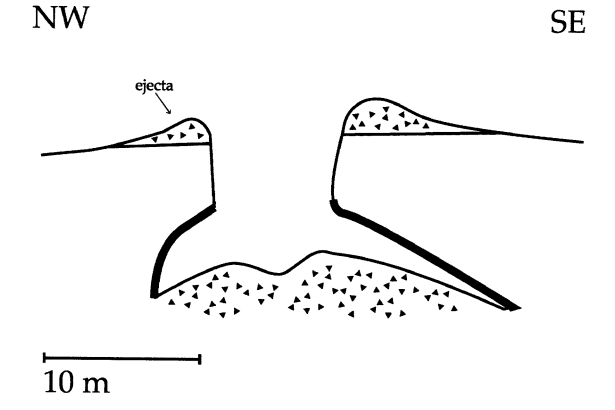


Fig. 7. Schematic cross section of cavity X. Bold black lines are cavity walls. Note antiformal profile. Modified from Jensen (1993).

The first three structural features (folds, vesicle lineations and flow banding) are features characteristic of fluid deformation, and are interpreted to form during viscous flow of lava during flow advance. In contrast, striations and chatter marks require plastic and brittle deformation, respectively, and thus record later (cooler) stages of deformation (although they are most likely also syneruptive). In this section we provide brief descriptions of these mesoscale structures. The orientations of the mesoscopic structures are then analyzed stereographically.

The inner walls of cavity structures are composed of flow-banded obsidian. Flow banding in rhyolitic lavas is defined by subplanar to planar variations in microlite and/or vesicle abundance. Common interior wall features include discrete, finely laminated, glassy plates (1–20 cm thick) that part from overlying layers along surfaces corresponding to flow banding, and mesoscopic folds (5–20 cm in wavelength; Fig. 8). Fold structures typically involve one or more flow layers (1–3 cm thick) that have been deformed into open folds as

obsidian layers translated past one another along small 'detachments'. Displacement along detachment planes may be marked by localized vesicular zones between layers.

Two types of linear structures are present within all cavities: (1) vesicle lineations, consisting of stretched and ruptured vesicles within the plane of flow banding; and (2) striations, or grooves in flow banding surfaces. Vesicle lineations are typically 10–50 mm in length and 2–5 mm wide. Vesicles deform during flow of the rhyolitic melt, and the long axis orientation reflects the local stretching direction or the axis of maximum extension (e.g. Taylor, 1932; Manga et al., 1998). Striations are best developed on the innermost surface of cavity A, where they are 20–500 mm in length and commonly parallel vesicle long axes (Fig. 9). Striations form as local asperities create grooves on flow layers that slide past one another.

Chatter marks are preserved in three of the four cavities surveyed, and are characterized by subparallel tension cracks 0.2–1 mm wide and 0.1–2 mm deep. Chatter marks are typically oriented at high angles to striations (Fig. 9b). While most common on the inner surfaces of the cavity walls, well developed chatter marks also occur beneath spalled off wall material in cavity A. The consistent orientation of chatter marks with respect to striations suggests that the two structures formed under similar stress regimes.

## 4.2. Structural analysis

Structural data from each cavity are plotted on lower hemisphere stereographic projections as poles to banding, trend and plunge of mesoscopic fold axes, and trend and plunge of lineations and striations (Fig. 10). Lineations and striations are labeled with the same symbol because they appeared parallel to each other in all cavities exam-

Table 1 Mesoscopic structures found in cavities

Cavity	Flow banding	Lineation	Folds	Chatter marks	Striations
A	$\sqrt{}$	$\sqrt{}$	$\checkmark$	$\checkmark$	√
G	$\checkmark$		$\checkmark$	$\checkmark$	$\checkmark$
SNJ	$\checkmark$	$\checkmark$	$\checkmark$		
X	$\sqrt{}$	$\sqrt{}$	$\checkmark$	$\checkmark$	$\checkmark$



Fig. 8. Steeply plunging mesoscopic multilayer folds in cavity A. Individual flow layers are approximately 5 cm thick. Contacts between layers are detachment surfaces.

ined. In each cavity examined, poles to banding plot on or near one or more great circles known as  $\pi$  circles. A  $\pi$  circle represents a plane that is exactly perpendicular to the hingeline of a fold (e.g. Davis, 1989). Thus, the pole to a  $\pi$  circle is the expression of a fold axis. Flow banding in cavities G and SNJ defines single  $\pi$  circles, each with a single pole. The  $\pi$  circle in cavity G is oriented N32W 46SW, with a corresponding fold axis oriented N58E 44 (Fig. 10a). In cavity SNJ, the  $\pi$  circle strikes N15W and dips 65NE and indicates a fold axis oriented S75W 25 (Fig. 10b). Flow banding in cavity X plots as two distinct clusters, each representing a group of measurements made on separate (northeast and southwest) cavity wall segments (e.g. Fig. 7). The scatter in banding measurements in the northwest wall reflects small-scale (~100 mm) crenulations that overprint the earlier deformation, which produced the large-scale fold structure. Crenulations were not evident in the southeast wall. Both groups of banding data can be fit by a single  $\pi$  circle oriented N67W 78SW, with a fold axis oriented N23E 12 (Fig. 10c).

Mesoscale structures in cavity A suggest a more complex structure than seen in the other cavities. Poles to flow banding plot within three distinct domains fit with three different  $\pi$  circles that indicate multiple fold axes (Fig. 10d). Domain 1 contains most of the points, and poles define a  $\pi$  circle which strikes N64E and dips 53NW. Domain 2 contains poles which define a  $\pi$  circle oriented N14W 48SW, while the third domain is characterized by a  $\pi$  circle oriented N06W 33NE. The cavity wall surfaces are smooth and devoid of the small-scale crenulations found in cavity X.

Linear structures preserved in cavity walls should also reflect conditions of flow. Lineations and striations in cavities G and SNJ trend approximately 90° from  $\pi$  circles and correlate well with stereographically deduced fold axes. Most



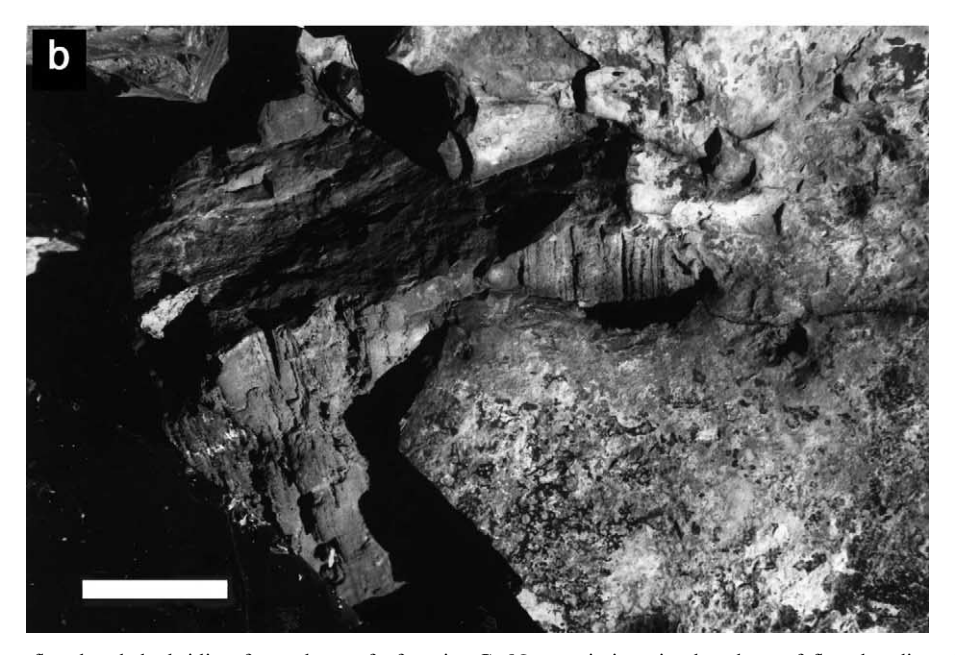


Fig. 9. (a) Platy flow-banded obsidian from the roof of cavity G. Note striations in the plane of flow banding. Chatter marks are oriented approximately normal to striations in the right side of the picture. Note boot in lower left corner for scale. (b) Close up view of striations in cavity G. Scale bar is 3 cm long.

lineations in cavity A also plot nearly perpendicular to the  $\pi$  circle defined by domain 1. Lineations in cavity X appear more scattered. The correlation between lineations and fold axes in

cavities G, SNJ, and A suggests that lineations and folds are coeval. Similarly, mesoscopic fold hinge orientations in cavities G and SNJ coincide with poles to  $\pi$  circles (i.e. they are coaxial with

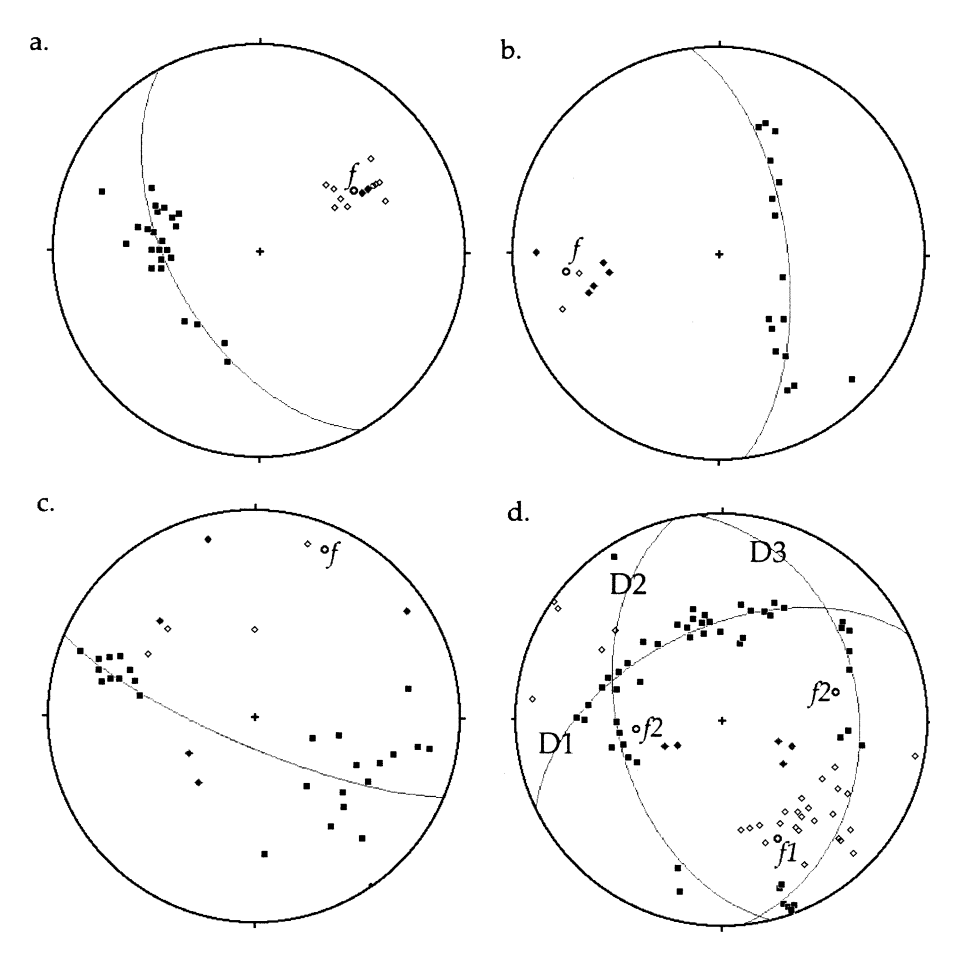


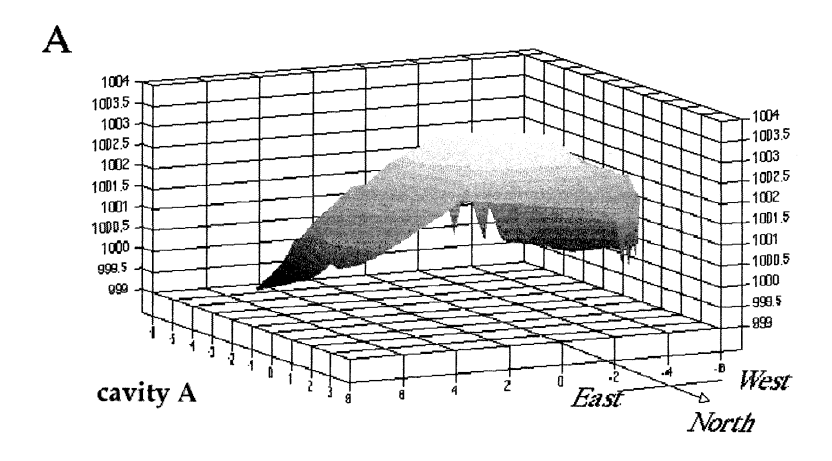
Fig. 10. Lower hemisphere stereographic projections of poles to flow layering (solid squares), lineations and striations (open diamonds), and mesoscopic fold axes (solid diamonds) in cavities (a) G, (b) SNJ, (c) X, and (d) A. Great circles are best fit representations of  $\pi$  circles. Open circles are poles to  $\pi$  circles and represent near-cylindrical fold axes. The scattered distribution of points in cavity X represents banding measurements from northwest-dipping cavity wall, while the relatively tight cluster of points represents flow bands forming the southeast-dipping cavity wall. In cavity A, flow banding forms three distinct domains (D1, D2, and D3) representing at least two folding events ( $f_1$ ,  $f_2$ ).

the inferred cavity fold axes), again, suggesting contemporaneous deformation. In cavities X and A, mesoscopic fold axes do not correlate with either poles to  $\pi$  circles or lineations.

## 4.3. Morphology of cavity A

Structural analysis of cavities X, G, and SNJ indicates that they have simple geometric fold shapes. Measurements of cavity A indicate a more complex shape, defined by multiple fold axes (Fig. 11). The cavity is approximately 11 m long by 8.5 m wide. It has an asymmetrical dome

shape with gently sloping southeast walls that become gradually steeper to the southwest and west (Fig. 11). The roof of the structure varies in height from about 3 cm in the southeast corner to approximately 250 cm in the northwest portion. The gently sloping southeast walls dip approximately 20° in the up-flow direction while the steeper southwest and west walls dip nearly 90° in the down-flow direction. Domain 1 lineations and striations oriented approximately parallel to the long axis of the cavity indicate that this domain reflects the overall structure of the cavity.



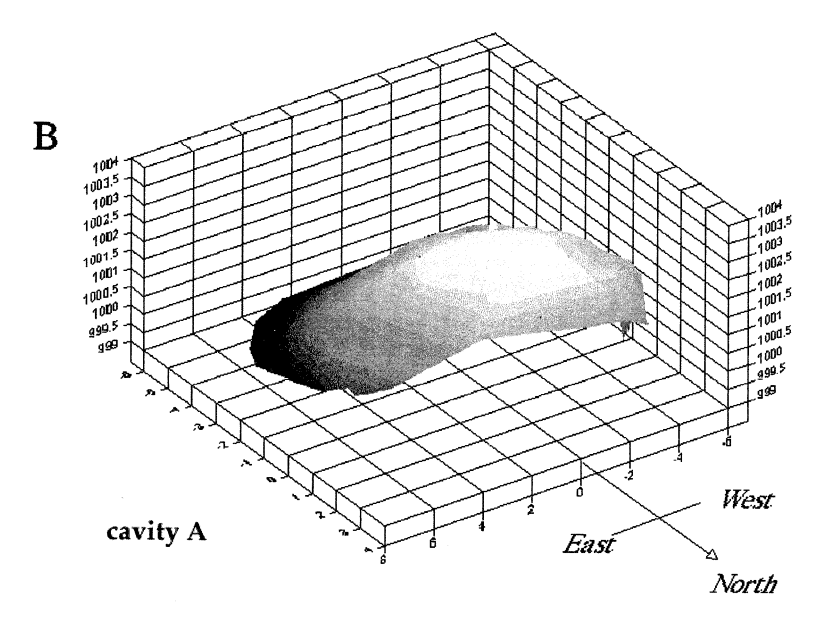


Fig. 11. Digital model of cavity A. Form is determined from 350 topographic measurements. (A) Northeast perspective. (B) Aerial perspective. Horizontal and vertical scales are in meters.

## 5. Discussion

## 5.1. Structural interpretation

The stereographic distribution of poles to flow banding in cavities X, G, and SNJ indicates that these cavities are near-cylindrical folds (e.g. Davis, 1989). Lineations and striations in cavities G, SNJ, and A plot approximately 90° away from their respective  $\pi$  circles and thus are coincident with fold axes. Mesoscopic fold orientations in

cavities G and SNJ are also parallel to cavity fold axes. Similarity in orientation between mesoscopic structures and cavity fold axes suggests that these structures are coeval. We interpret lineations and striations to represent the local stretching direction, as they are oriented perpendicular to the maximum shortening direction inferred from cavity fold axis orientations.

Flow banding in cavity A is more variable, as poles plot within three distinct domains, each forming a unique  $\pi$  circle. Thus the macroscopic

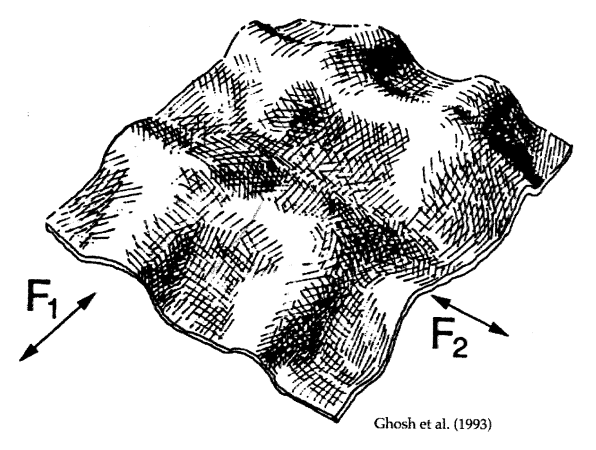


Fig. 12. Illustration of a superposed deformation experiment conducted by Ghosh et al. (1993). Domal, non-cylindrical folds were produced by shortening early formed folds  $(f_1)$  about an axis  $(f_2)$  oriented nearly perpendicular to  $f_1$ .

structure of cavity A is that of a refolded fold, with each flow banding domain representing a unique fold axis. The fold axes indicate at least two folding events. An initial phase of shortening produced the single, near-cylindrical fold (f<sub>1</sub>) represented by data in domain 1. A second buckling event, superposed at high angles to f1, produced two later folds (f<sub>2</sub>) oriented nearly 90° to the earlier formed fold (represented by domains 2 and 3; Fig. 10). The f<sub>2</sub> folds trend approximately 180° from one another. The steep down-flow wall in cavity A suggests that after initial buckling, the flow continued to the northwest, rotating the f<sub>1</sub> fold into its present position. Single-layer buckling experiments by Ghosh et al. (1993) show that this sequence of deformation forms open folds with domal shapes similar to the measured shape of cavity A (Fig. 12).

Cavity structure orientations are compatible with surface fold orientations. Fig. 13 shows fold axes for each cavity structure plotted on a

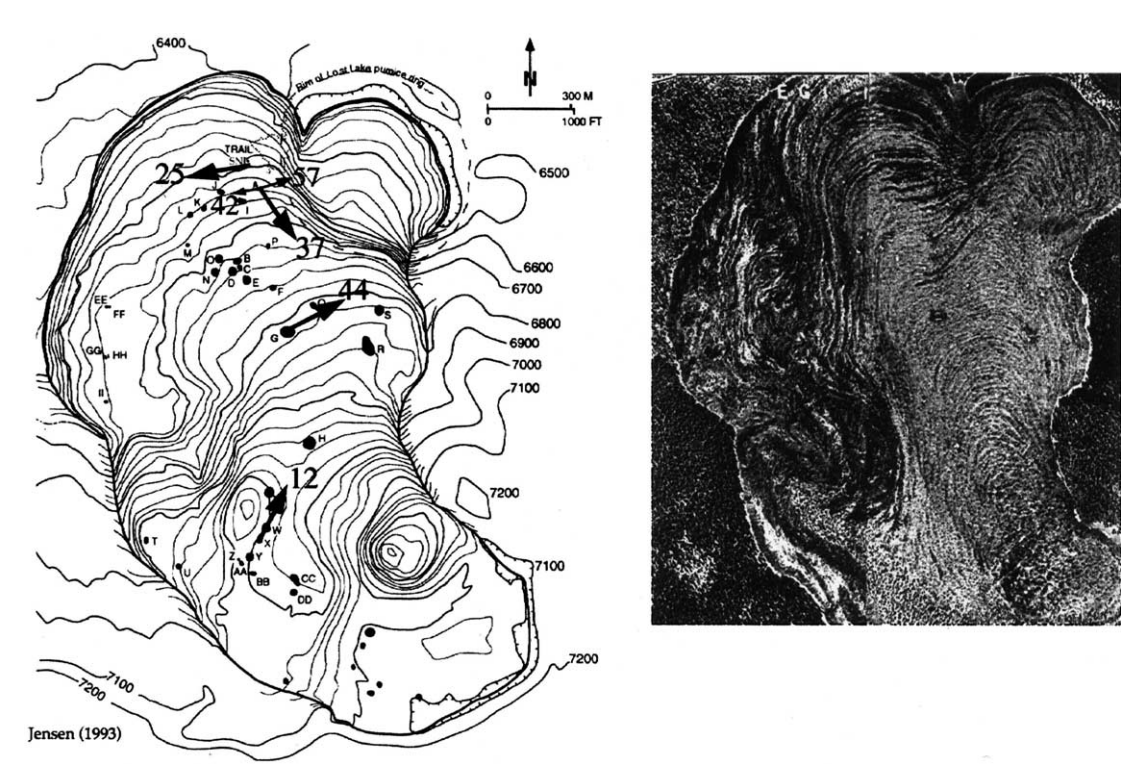


Fig. 13. Topographic map and aerial photo mosaic of the Big Obsidian Flow showing fold axis orientations in cavities. Numbers at tips of arrows indicate the plunge of cavity fold axes. Letters on aerial photograph mark the approximate locations of cavity structures. Note that fold axes trend normal to the flow direction inferred from the orientation of flow ridges.

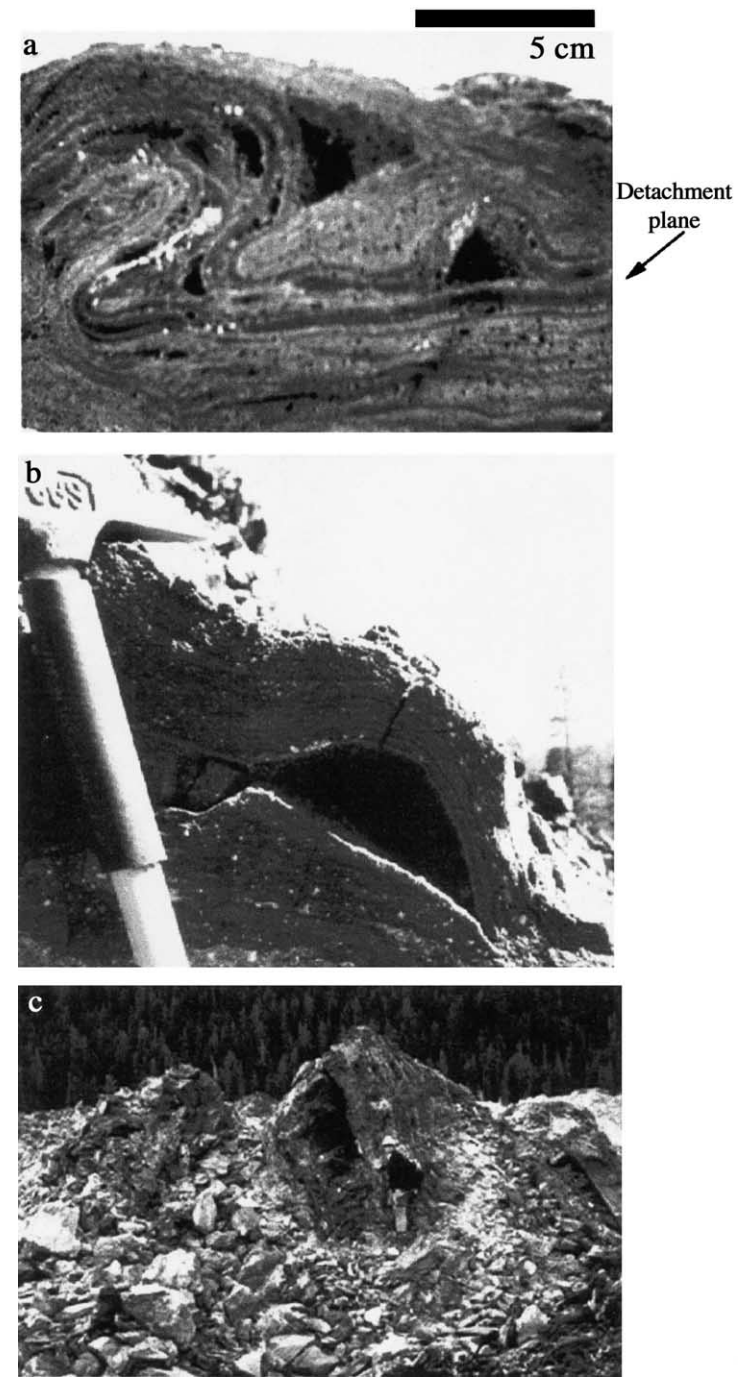


Fig. 14. (a) Mesoscopic pull-apart fold in interlayered obsidian and pumice. A small cavity ( $\sim$ 2 cm) formed in the hinge of the fold as the folded layer slid along a detachment plane. (b) Pull-apart fold ( $\sim$ 10 cm) with associated small cavity in Obsidian Dome, CA, USA. (c) Buckle folds on the surface of Big Glass Mountain, CA, USA. Note  $\sim$ 1.5 m tall cavity in the hinge region.

topographic map of the Big Obsidian Flow. Flow directions are interpreted to be normal to the axes of compressional flow ridges. Cavity X is located between the vent and a prominent topographic high in a zone where several flow ridges trend approximately N05E. The stereographically determined fold axis of cavity X (N23E 12) is subparallel to this flow ridge direction. These ridges probably formed as lava flowing from the vent was buttressed to the northwest by a topographically high lava mound down-slope from the vent (Williams, 1935). Cavity G is located in the middle of a flow ridge trending approximately N70E, which is subparallel to the fold axis (N58E 44) indicated by flow layering measurements. Cavity A lies within a coarse pumice flow ridge trending approximately N35W which is subparallel to the f<sub>1</sub> fold axis (S25E 37). Cavity SNJ shows a similar correspondence of fold axis (S75W 25) orientation with surface ridge geometry (N80W). Alignment of cavity fold axes with large surface ridges indicates that cavities form as a consequence of flowrelated deformation and not by buoyancy-driven deformation (e.g. Jensen, 1993).

### 5.2. Folding mechanism

Structural relations suggest that cavities form near the flow surface by a buckling mechanism. Buckling occurs because the upper part of the flow is cool and stiff relative to the flow interior and, owing to this large viscosity contrast, the flow 'crust' assumes the compressive load (e.g. from a topographic barrier or a reduced slope). Buckle folds grow as the flow progressively shortens. Viscous deformation in the flow interior may lead to further thickening of the flow.

Fink (1980) estimated the thickness of the rigid surface crust on the Big Glass Mountain flow to be approximately 10–15 m based on measurements of fracture depth within the flow and analysis of surface fold spacing. The dominant surface fold wavelength, measured as the arc wavelength, is controlled by the buckled layer thickness (rigid crust) and the ratio of viscosity of the crust to that of the flow interior (e.g. Fink and Fletcher, 1978). Surface folds measured on aerial photographs of the Big Obsidian Flow have a mean

spacing of  $25 \pm 10$  m. The amplitudes of these folds are small (1-2 m) compared to their wavelengths, thus apparent wavelength gives a close approximation of their arc wavelength (Green and Short, 1971). This spacing is ~15 m less than the average spacing of folds on Big Glass Mountain (Fink, 1980). For similar viscosity profiles, the observed difference in mean fold spacing reflects different crust thicknesses, suggesting that the crust on the Big Obsidian Flow was somewhat thinner at the time of buckling than the 10-15 m thick crust at Big Glass Mountain. A maximum crust thickness of ~10 m is consistent with the depths of cavities A, X, G, and Z (Jensen, 1993). That cavity SNJ is exposed at a depth of only a few meters suggests that buckling and resulting cavity formation occur throughout the upper 10 m of the flow.

Cavity formation during buckling requires weak surfaces along which slip and layer separation (pull-apart) can occur. Shear strain localized along the interface between the deforming crust and the more fluid interior may form these detachment surfaces. Since the upper surface of the flow is unconfined, folds grow vertically and, with continued shortening, the crust separates from the flow interior to form a cavity. Cavities may also form within shallower parts of the buckled crust where shortening leads to separation of individual flow layers along fold hinges (e.g. SNJ). In the context of this model, cavity floors and walls are detachment planes along which layer-parallel slip and separation occurs. While direct evidence for basal detachment surfaces is obscured by talus on the floors of all cavities, striations and lineations on cavity walls provide evidence of a slip surface.

This folding mechanism also occurs on a smaller scale in the form of mesoscopic pull-apart folds, which are ubiquitous in obsidian flows. Fig. 14 shows examples of pull-apart folds in Big Glass Mountain, CA, USA, in which void space was created in their hinge zones. In the first example, a deformed series of alternating glassy and pumiceous layers shows a well developed cavity in the hinge zone of a small fold (2-cm wavelength). The fold, composed of obsidian, penetrated and deformed the overlying pumiceous

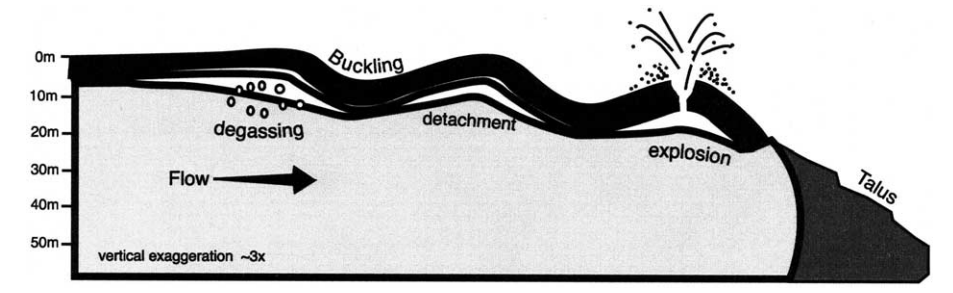


Fig. 15. Schematic model of the formation of gas cavities and explosion craters. Buckling of the upper surface causes crust to detach from the flow interior. Individual flow layers within the crust may also pull apart. Cavities formed in hinge zones trap magmatic and meteoric volatiles prior to explosion. Scale is approximate.

lava as it translated along a basal detachment surface. The overlying pumiceous lava is both less dense and less viscous than the folded obsidian layer and thus it provided little resistance to growth of the fold (e.g. Castro and Cashman, 1999). Larger, structurally similar cavities are shown in Fig. 14b,c.

# 5.3. Implications for explosive activity on the Big Obsidian Flow

The close association of cavity structures and

explosion craters on obsidian flows indicates that cavities play an important role in surficial explosive activity. Fig. 15 depicts a schematic model showing the formation of cavity structures in the shallow crust and their relation to endogenous explosions. According to this model, cavities serve as reservoirs for exsolved magmatic and/or meteoric water. When the vapor pressure in the cavity exceeds the strength of the surface crust, an explosion results. In the simplest scenario, the volatiles are purely magmatic. DeGroat-Nelson et al. (2001) find that magmatic volatile concentrations

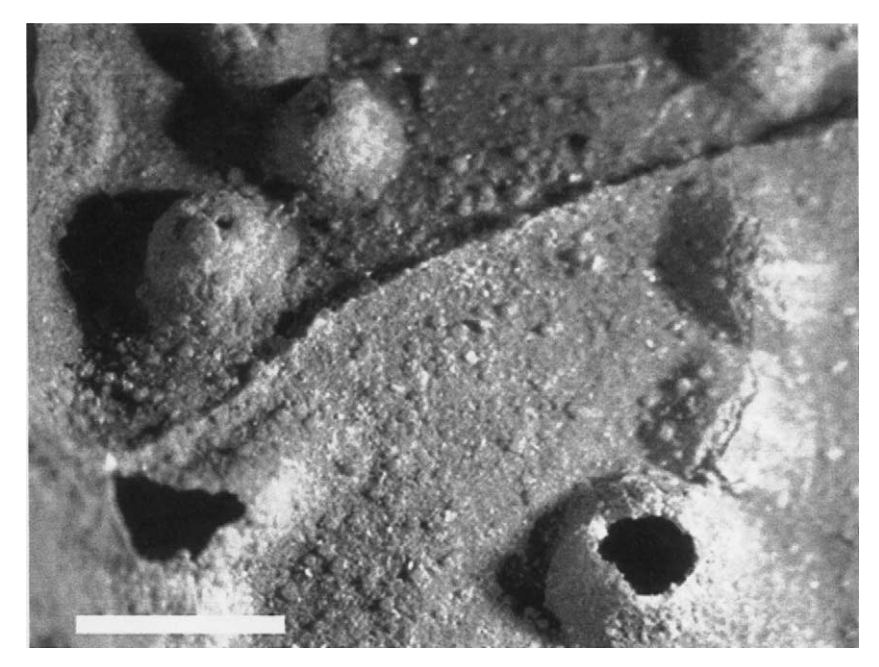


Fig. 16. Small vesicles protruding into cavity X (scale bar  $\sim$  3 mm). These features may record gas diffusion into the cavities in response to a local pressure decrease accompanying cavity formation.

at depths of 10–20 m in obsidian flows are high enough to produce gas pressures in excess of estimated surface crust strengths (e.g. Fink and Griffiths, 1998). This depth is consistent with the average depth of both explosion craters and cavity structures on the Big Obsidian Flow.

The simple model above requires that a cavity be airtight upon formation, as suggested by the dense glassy selvages that line the walls of every cavity. If cavities are closed to the atmosphere, layer separation (volume increase) would produce a chamber under vacuum rather than at positive pressure. The pressure difference between the cavity and surrounding lava would induce diffusion of magmatic volatiles into the cavity. Walls of cavities commonly contain evidence of bubble mi-

gration, growth, and rupture into cavities (Fig. 16). While subsequent cooling would reduce the pressure of gas within the cavity, it would also promote crystallization in the flow interior, with the potential for additional gas transport into the cavity (e.g. Fink and Manley, 1987). Prior to venting, cavity wall strength balances the pressure within the cavity. Motion of the flow after the cavity becomes pressurized may destabilize the cavity and a gas explosion may occur as the crust is broken.

Alternatively, a cavity may be partially connected to the atmosphere, such that the cavity could have fluids introduced from both magmatic and meteoric sources. In this scenario, pressure gradients arising from detachment are balanced



Fig. 17. Explosion craters on the surface of the Big Obsidian Flow. Crater alignments, consisting of two or more craters positioned in close proximity to antiformal ridges, are evident in the northern, central, and southern parts of the flow. Scale bar represents approximately 300 m.

by fluid flow into the cavity. Meteoric water (e.g. rain or snow melt) may enter the cavities through microcracks and fractures. Mechanical mixing of this water with the still hot flow interior may result in the water flashing to steam, thus increasing the pressure in the cavity. Explosions may occur if steam escape is periodically blocked (Mastin, 1995) or if the rate of steam expansion outpaces the rate at which it bleeds off the cavity. Moyer and Swanson (1987) described a similar steam blast phenomenon in pyroclastic flows at Mount St. Helens following the 18 May and 12 June eruptions.

It is likely that both mechanisms (closed and open) drive explosions from the surface of obsidian flows. From a hazards perspective, the main reason to study cavity structures is to identify the areas on the flow that are prone to explosion. Whether the source of explosion is magmatic or meteoric vapor, cavities provide a local trap for volatiles and thus control the locations of explosions. Physical evidence of this process is shown by explosion crater alignments (Fig. 17). On the northern flow lobe, four craters are aligned parallel to the trend of a continuous flow ridge. Crater alignments are also apparent near the vent, in the central and south-central flow, and in the far western part of the flow. Similar crater alignments exist on the south lobe of Big Glass Mountain (e.g. Green and Short, 1971). In most cases, explosion craters lie near or on surface ridges. These relations suggest that cavities are most likely to vent on the axes of antiformal ridges, where extensional strain is the greatest. The alignments are evidence that explosive activity is structurally controlled.

#### 6. Summary

Analysis of small-scale structures in the Big Obsidian Flow, OR, USA, suggests a structural mechanism for the formation of giant gas cavities in obsidian flows, and lends insight into the mechanisms that control explosive activity on silicic lava flows. Stereographic relations of flow banding, lineations, striations, and mesoscopic fold axes indicate that most cavities are near-cylindri-

cal and non-cylindrical folds. Cavity fold axes align with large-scale compressional flow ridges, suggesting that cavities form during flow advance as the upper 5-10 m (i.e. the approximate depth of cavities in explosion craters) of the flow buckles. Cavities form under the following conditions: (1) the flow surface is cool and stiff, and thereby responds to the compressive load by buckling; (2) layer separation occurs along detachment planes, either along the base of the crust or within the crust between individual flow layers. The position of detachment planes may be governed by the distribution of relatively low viscosity bubbly lava within the flow (e.g. Fink and Manley, 1987), as these layers are weak compared to bubble free lava (e.g. Manga et al., 1998). Recognition of cavity structures on both macroscopic and mesoscopic scales suggests that pull-apart folding is common throughout the upper 10 m of obsidian flows. Once formed, cavities serve as reservoirs for exsolved magmatic and meteoric volatiles and, as the pressure within cavities exceeds the strength of the overlying lava, they vent explosively to form craters on the flow surface. The link between cavity formation and explosive activity therefore suggests that surface explosions may occur during flow emplacement. Quantifying explosive timing and potential in future obsidian dome eruptions will require additional studies of craters on the surfaces of other well preserved flows (e.g. Big and Little Glass Mountain, CA, USA, Rock Mesa, OR, USA).

## Acknowledgements

This work was supported by a GSA grant-in-aid of research to J.C., and NSF EAR-9614753 to K.C. Special thanks to D. Sahagian for a thoughtful review. The authors also greatly acknowledge the comments of an anonymous reviewer and Robert Jensen for helpful discussions during the preparation of this manuscript.

#### References

Castro, J.M., Cashman, K.V., 1999. Constraints on rheology

- of obsidian and pumice based on folds in obsidian lavas. J. Struct. Geol. 21, 807–819.
- Chitwood, L.A., Jensen, R.A., 2000. Large prehistoric flood along Paulina Creek, Newberry Volcano, Oregon. In: Jensen, R.A., Chitwood, L.A., (Eds.), What's New at Newberry Volcano, Oregon. 8th Annual Friends of the Pleistocene Field Trip Guidebook. pp. 32–40.
- Davis, G., 1989. Structural Geology of Rocks and Regions. John Wiley and Sons, New York.
- DeGroat-Nelson, P.J., Cameron, B.I., Fink, J.H., Holloway, J.R., 2001. Hydrogen isotope analysis of rehydrated silicic lavas: implications for eruption mechanisms. Earth Planet. Sci. Lett. 185, 331–341.
- Fink, J.H., 1980. Surface folding and viscosity of rhyolite flows. Geology 8, 250–254.
- Fink, J.H., 1983. Structure and emplacement of a rhyolitic obsidian flow: Little Glass Mountain, Medicine Lake Highland, northern California. Geol. Soc. Am. Bull. 94, 362–380.
- Fink, J.H., Anderson, S.W., Manley, C.R., 1992. Textural constraints on silicic volcanism: beyond the permeable foam model. J. Geophys. Res. 97, 77–88.
- Fink, J.H., Fletcher, R.C., 1978. Ropy pahoehoe: Surface folding of a viscous fluid. J. Volcanol. Geotherm. Res. 4, 151–170.
- Fink, J.H., Griffiths, R.W., 1998. Morphology, eruption rates, and rheology of lava domes: Insights from laboratory models. J. Geophys. Res. 103, 527–545.
- Fink, J.H., Manley, C.R., 1987. Origin of pumiceous and glassy textures in rhyolite flows and domes. In: Fink, J.H. (Ed.), The Emplacement of Silicic Domes and Lava Flows. Geol. Soc. Am. Spec. Pap. 212, 77–89.
- Fink, J.H., Manley, C.R., 1989. Explosive volcanic activity generated within advancing silicic lava flows. In: Latter, J. (Ed.), Volcanic Hazards. International Association of Volcanology and Chemistry of the Earth's Interior Proceedings in Volcanology 1, 169–179.
- Ghosh, S.K., Mandal, N., Sengupta, S., 1993. Superposed buckling in multilayers. J. Struct. Geol. 15, 95–111.

- Green, J., Short, N.M., 1971. Volcanic Landforms and Surface Features. Springer, New York.
- Hon, K., Denlinger, R., Kauahikaua, J., Mackay, K., 1994. Emplacement and inflation of pahoehoe sheet flows; observations and measurements of active lava flows on Kilauea Volcano, Hawaii. Geol. Soc. Am. Bull. 106, 351–370.
- Jensen, R.A., 1993. Explosion craters and giant gas bubbles on Holocene rhyolite flows at Newberry Crater, Oregon. Oregon Geol. 55, 13–19.
- MacLeod, N.S., Sherrod, D.F., Chitwood, L.A., 1982. Geologic map of Newberry Volcano, Deschutes, Klamath, and Lake Counties, Oregon. U.S. Geol. Surv. Open-File Report 82-847.
- Manga, M., Castro, J.M., Cashman, K.V., Loewenberg, M., 1998. Rheology of bubble-bearing magmas. J. Volcanol. Geotherm. Res. 87, 15–28.
- Mastin, L.G., 1995. Thermodynamics of gas and steam-blast eruptions. Bull. Volcanol. 57, 85–98.
- Moyer, T.C., Swanson, D.A., 1987. Secondary hyrdroeruptions in pyroclastic-flow deposits: examples from Mount St. Helens. J. Volcanol. Geotherm. Res. 32, 299–319.
- Nakada, S., Miyake, Y., Sato, H., Oshima, O., Fujinawa, A., 1995. Endogenous growth of dacite dome at Unzen volcano Japan. Geology 23, 157–160.
- Robinson, S.W., Trimble, D.A., 1983. US Geological Survey, Menlo Park, California, radiocarbon measurements III. Radiocarbon 25, 143–151.
- Russell, I.C., 1905. Preliminary report of the geology and water resource of central Oregon. U.S. Geol. Surv. Bull. 252, 138 pp.
- Smith, J.V., Houston, H.C., 1994. Folds produced by gravity spreading of a banded rhyolite flow. J. Volcanol. Geotherm. Res. 63, 89–94.
- Taylor, G.I., 1932. The viscosity of a fluid containing small drops of another fluid. Proc. R. Soc. London A 138, 41–48.
- Williams, H., 1935. Newberry volcano of central Oregon. Geol. Soc. Am. Bull. 46, 253–304.